THE POTENTIAL OF MULTI-MATERIAL LASER POWDER BED FUSION ILLUSTRATED BY AN RFQ PROTOTYPE

M. Mayerhofer*[1], S. Brenner[1], G. Dollinger[1], C. Jugert[2],
M. Lehmann[2], V. Nedeljkovic-Groha[1], G. Schlick[2]
[1]University of the Bundeswehr Munich, Neubiberg, Germany
[2]Fraunhofer Institute for Casting, Composite and Processing Technology, Augsburg, Germany

Abstract

A variety of studies have shown that additive manufacturing (AM) of particle-accelerator components using laser powder bed fusion (PBF-LB/M) offers significant potential to reduce investment costs while simultaneously improving figures of merit. However, the classical PBF-LB/M process does not support the combination of different materials within a single part. Conventional manufacturing routines are therefore still required, for example, to join steel flanges with knife-edge sealing interfaces to copper cavities. Novel multi-material (MM) PBF-LB/M processes enable the fabrication of high-quality, e.g., high-density, geometries by combining different materials such as Cu, CuCr1Zr, Ta, W, aluminium alloys, or stainless steel. Highly functional parts tailored to the diverse requirements of particle-accelerator components can thus be additively manufactured within a single process step. To demonstrate this potential, we fabricated a monolithic radio-frequency quadrupole (RFQ) prototype from two materials using MM PBF-LB/M. The RFQ inner cavity was manufactured from CuCr1Zr, while the co-printed outer shell was made of tool steel to integrate two DNCF63 and four DNCF16 flanges. The inner cavity surface was electropolished and subsequently copper plated to increase the cavity quality factor. Low-level RF measurements showed good agreement with CST simulations when the remaining surface roughness was taken into account. Helium leak-rate measurements demonstrated vacuum performance compatible with conventional RFQ applications. For the first time, these results demonstrate the feasibility of MM PBF-LB/M for manufacturing functional multi-material particle-accelerator components.

POTENTIAL OF MULTI-MATERIAL LASER POWDER BED FUSION

Laser powder bed fusion of metals (PBF-LB/M) is an additive manufacturing process in which thin metal powder layers are selectively melted by a laser to build components layer by layer. This enables complex monolithic geometries that are difficult or impossible to realize conventionally. For particle-accelerator components, such as radio-frequency (RF) cavities, PBF-LB/M is therefore of increasing interest to reduce manufacturing effort and cost while improving performance, for example through integrated cooling channels or topology-optimized structures [1–5].

* michael.mayerhofer@unibw.de

However, conventional mono-material PBF-LB/M remains limited when different material properties are required within one component. In normal conducting RF cavities, for instance, the cavity body is typically made from highly conductive copper or copper alloys, whereas vacuum interfaces often require stainless-steel knife-edge flanges. Such assemblies still rely on conventional joining processes, which increase manufacturing complexity, restrict design freedom, and may introduce additional cost and failure risks. Multi-material PBF-LB/M addresses this limitation by enabling the layer-wise fabrication of components composed of different metals within a single process [6, 7]. Functional requirements such as high electrical conductivity, mechanical robustness, thermal management, and vacuum compatibility can thus be combined directly in one additively manufactured structure. MM PBF-LB/M can therefore reduce or even eliminate conventional joining steps and further expand the design freedom for particle-accelerator components composed of different materials. Several MM PBF-LB/M processes are currently under development, and for selected material combinations the technology has reached a maturity level that allows the fabrication of functional prototypes. For example, at Fraunhofer IGCV a MM PBF-LB/M process for producing high-quality multi-material components was developed [8].

Figure 1 summarizes material combinations already processed by MM PBF-LB/M that may be relevant for particle-accelerator applications. Given the rapidly growing research activity in this field, the overview is not exhaustive. The numbers in the fields refer to the corresponding literature references. The color code distinguishes material combinations investigated in initial studies, qualified at laboratory scale, and demonstrated in application-specific prototypes. One such prototype is the RFQ demonstrator first presented in Brenner et al. [9]. It combines a CuCr1Zr inner RF cavity with a co-printed tool-steel outer structure containing integrated CF knife-edge flanges (see Fig. 2).

RFQ PROTOTYPE

Design and MM PBF-LB/M Process

The potential of single-material PBF-LB/M for manufacturing RF cavities from pure copper has already been demonstrated [1–5]. However, pure copper is challenging for realizing vacuum-tight knife-edge sealing interfaces. Therefore, most PBF-LB/M-manufactured RF cavities

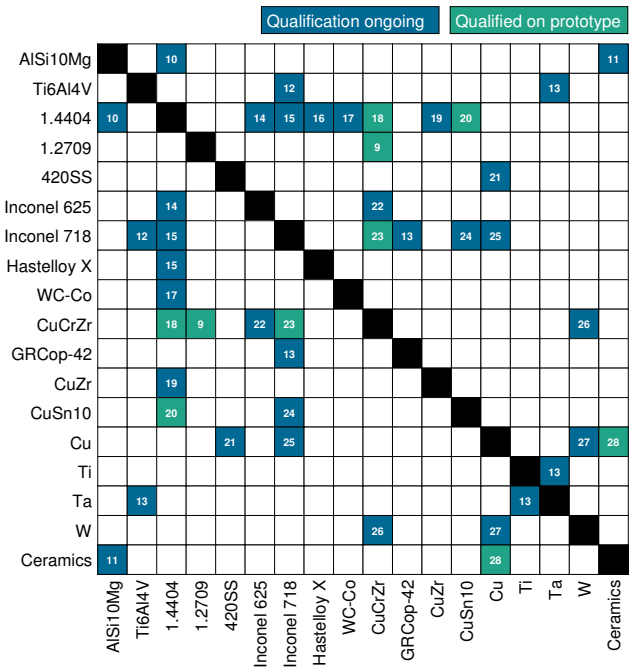

Figure 1: Matrix of reported MM PBF-LB/M material combinations that may be relevant for the fabrication of particle-accelerator components.The numbers in the fields refer to the corresponding literature references.

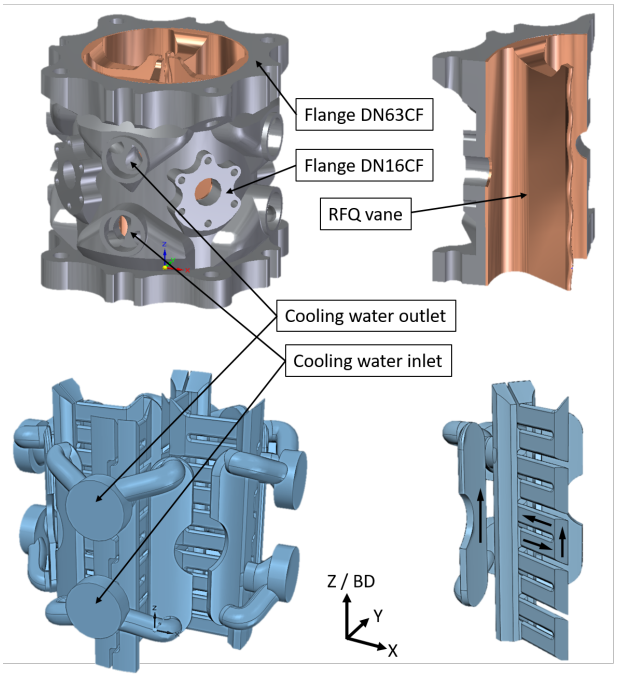

Figure 2: CAD model of the complete RFQ prototype and a single RFQ quadrant, including the negative geometry of the integrated cooling channels.

relied on Viton O-ring seals, limiting their applicability in, for example, high radiation environments.

The RFQ prototype shown in Fig. 2 was designed to demonstrate that MM PBF-LB/M can overcome this limitation. The inner RF cavity was manufactured from an electrically conductive copper alloy (CuCr1Zr), while the mechanically robust outer structure, including the knife-edge sealing flanges, was co-printed from tool steel (1.2709). The RFQ geometry was developed using CST Microwave Studio and Ansys Workbench 2024 R2. The prototype follows a four-vane RFQ design and is equipped with DN63CF flanges at both ends for connection to further RFQ sections or integration into a beamline. Four additional DN16CF flanges provide interfaces for diagnostics, vacuum components, or electromagnetic field manipulation. Each RFQ quadrant contains an individual cooling circuit running through the vane and outer shell (see Fig. 2).

Manufacturing was performed using a customized SLM 280HL system (Nikon SLM Solutions AG) with separate recoating and suction units for the two materials, as described by Anstaett [8]. Figure 3a shows the RFQ after PBF-LB/M, still surrounded by powder. Figure 3b shows the prototype after CNC machining of the knife-edge sealing interfaces. The available build volume of the MM PBF-LB/M system, 95 mm × 95 mm × 91 mm in x-, y-, and z-direction, limited the maximum RFQ dimensions and resulted in a CST-simulated resonance frequency of 1402 MHz for the TE_{210} mode. Since pure copper could not yet be processed with steel alloys on the system used, the outer structure was manufactured from tool steel (1.2709), while the inner cavity was manufactured from CuCr1Zr. Compared with pure copper, CuCr1Zr exhibits at least 20% lower bulk electrical conductivity, which reduces the expected RF quality factor [30]. The quality factor is further limited by the intrinsic surface roughness of PBF-LB/M parts (typically $Sq > 10$ µm), making post-processing of the inner RFQ surfaces necessary. After MM PBF-LB/M fabrication, the printed part was blasted, and depowdered.

Two-Step Post-Processing

In previous studies, we demonstrated that chemical post-processing can increase the quality factor of PBF-LB/M-manufactured RF cavities to up to 97% of the CST-simulated value [5, 29]. At the same time, the chemical post-processing enabled precise resonance-frequency tuning to within ±0.8 MHz. Other studies have investigated tumbling, plasma electrolytic polishing, and coating to reduce RF cavity surface roughness. However, to the best of our knowledge, either material-removing or material-depositing processes where applied [4].

For RFQs, the complex internal geometry makes uniform material removal or deposition particularly challenging and non-uniform surface modification can alter the electromagnetic field distribution. Therefore, we decided to apply a two-step post-processing. The RFQ and a four-finger metallic counter-electrode, with one finger assigned to each RFQ quadrant, formed an anode-cathode arrangement connected to a rectifier. First, electropolishing was performed with the RFQ acting as the anode. The electrolyte Poligrat E 104 (Poligrat GmbH), developed for copper and copper-alloy

surfaces, was used. Approximately 10 m of material was removed from the inner surface to reduce roughness. Second, the polarity was reversed, such that the RFQ acted as the cathode, and pure copper was electrodeposited from a sulfuric-acid-based copper electrolyte. The target copper layer thickness was approximately 10 m to further reduce surface roughness. Since the same electrode arrangement is used in both steps, similar electric field distributions are to be expected; consequently, balancing material removal and deposition may make it possible to maintain the original geometry. Figures 3c and 3d show the RFQ during and after post-processing, respectively.

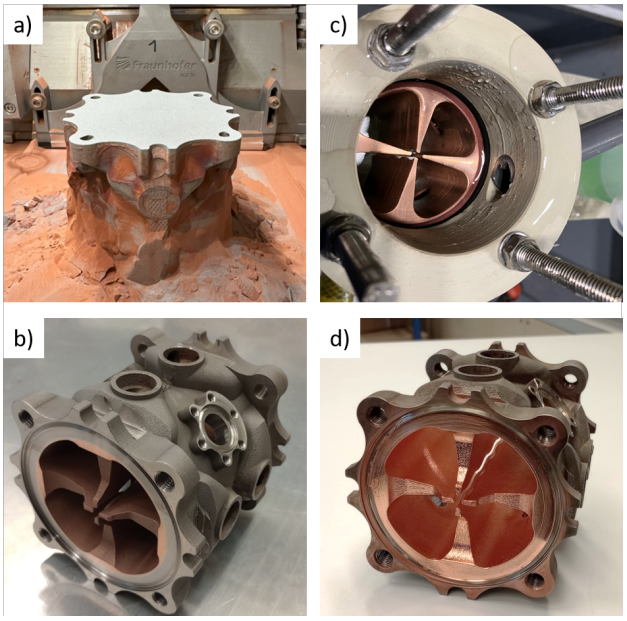

Figure 3: RFQ prototype: (a) after MM PBF-LB/M and still surrounded by powder, (b) after CNC machining of the knife-edge sealing interfaces, (c) during post-processing, and (d) after post-processing.

Low-Level RF Measurements

Low-level RF measurements were performed using a Siglent SNA5012A vector network analyzer with two inductive loop probes in a S_{21} measurement under weak coupling conditions ($\beta \ll 1$). The probes were mounted on two opposing DN16CF flanges. The measurement setup and a representative S_{21} spectrum of the TE_{210} mode are shown in Fig. 4a and 4b, respectively.

The measured unloaded quality factors before and after post-processing were approximately 1100 and 3100, respectively. The increase of nearly 200% is attributed to the reduced surface roughness achieved by post-processing. Compared with the CST-simulated value of approximately 4100, the measured quality factor remains reduced by about 25%. When the remaining surface roughness of the RFQ prototype ($R_q \approx 3.6$ m) is included in the CST simulations, a quality factor of approximately 2800 is obtained, which is close to the measured value.

The measured resonance frequencies before and after post-processing were 1417 MHz and 1436 MHz, respectively. Compared with the CST-simulated resonance frequency of 1402 MHz, the as-built RFQ already shows an increase of 15 MHz, which is further increased by 19 MHz after post-processing. Thus, full compensation between material removal during electropolishing and material deposition during copper plating was not achieved. However, compared with additively manufactured RFQ prototypes in which surface roughness is reduced exclusively by material removal, the relative post-processing-induced frequency shift is reduced by approximately a factor of seven [31]. The two-step approach therefore appears promising, although further optimization is required to maximize the quality factor while maintaining the resonance frequency.

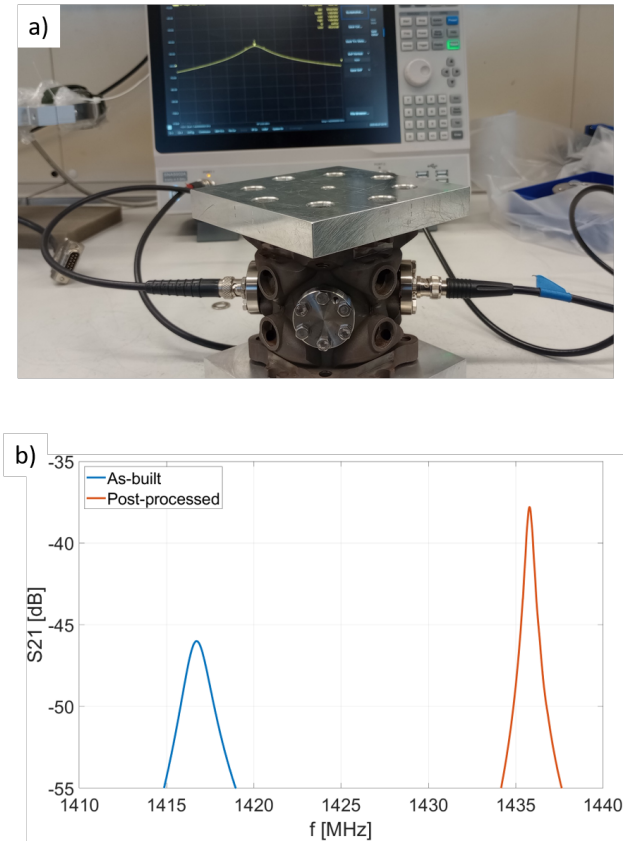

Figure 4: (a) Low-level RF measurement setup. (b) S_{21} spectrum of the TE_{210} mode for the as-built and post-processed RFQ prototype.

Helium Leak Rate

The experimental setup for helium leak rate measurement is shown in Fig. 5a. The RFQ prototype was sealed with four CF flanges and copper gaskets and evacuated using a scroll pump. The sealed prototype was then transferred into a plastic container holding a saturated ^{4}He atmosphere. Inside this container, the prototype was opened, filled with ^{4}He, and sealed again. For the leak-rate measurement, the

helium-filled RFQ prototype was placed inside a DN160CF vacuum pipe section, which was sealed with CF flanges and connected to a Pfeiffer ASM340DRY helium leak detector for measurement of the integral helium leak rate.

The measured helium leak rate is shown in Fig. 5b. The ^{4}He leak rate decreased to below $6 \cdot 10^{-8}$ mbar L s^{-1} and tended toward a lower limit. Scaled to an RFQ length of 1 m and assuming a pumping speed of 100 mbar L s^{-1}, corresponding to a standard CF100 turbomolecular pump, an internal pressure of at least $1 \cdot 10^{-8}$ mbar can be achieved. This pressure level is sufficient for many conventional RFQ applications.

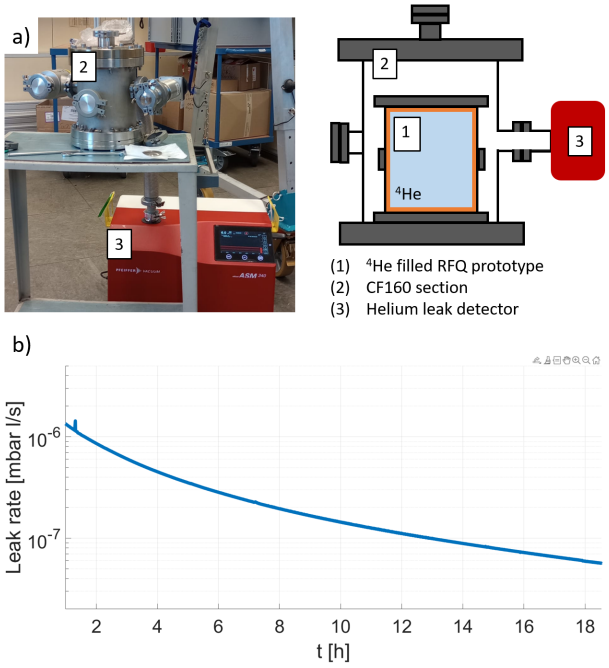

Figure 5: Integral helium leak-rate measurement: (a) experimental setup and (b) measured ^{4}He leak rate over time.

Nevertheless, the RFQ prototype exhibits a helium leak rate at least two orders of magnitude higher than reported for additively manufactured copper membranes [4]. Based on microscopic images of the x-y material-transition zone, shown in Fig. 6a, the elevated leak rate cannot be attributed to a network of connected cracks, as previously assumed in [9].

A possible explanation is the presence of powder residues inside the cooling channels, as shown in Figs. 6b and 6c. These residues form a porous volume in which ^{4}He may have been trapped during ^{4}He filling and gradually released during the leak test. This could explain both the apparently increased helium leak rate and the observed decrease of the leak-rate signal over time.

Powder adhesion in complex geometries is a well-known issue for PBF-LB/M parts. Complete removal of residual powder from internal channels should therefore receive greater attention in future studies. CT imaging may be suitable to verify powder removal and identify remaining residues.

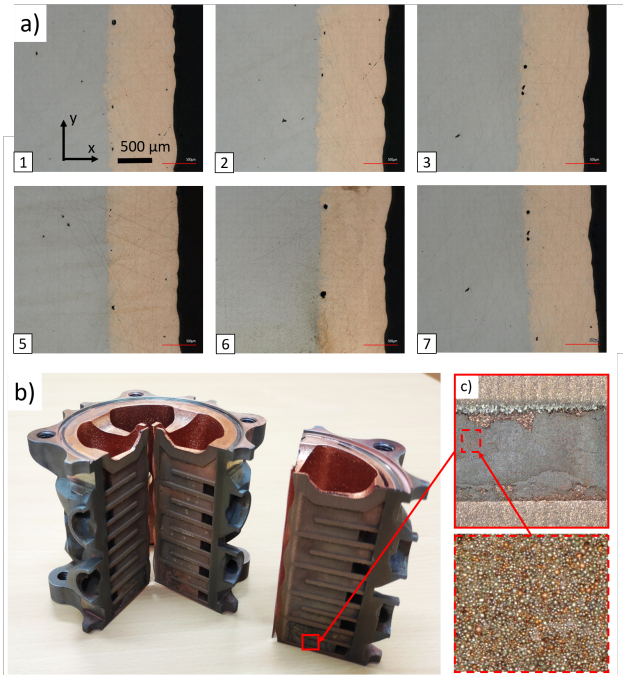

Figure 6: (a) Microscopic images of the *xy* material-transition zone. (b, c) Powder residues inside the cooling channels.

CONCLUSION

Multi-material PBF-LB/M enables components from different materials to be fabricated within a single manufacturing step and can therefore reduce the need for conventional joining processes. Compared with conventional manufacturing and mono-material PBF-LB/M, this further expands the design freedom of functional accelerator components. For PBF-LB/M manufactured RF cavities, for example, the integration of stainless-steel knife-edge vacuum flanges currently represents a design limitation and adds manufacturing effort, as it typically requires joining processes such as brazing.

To demonstrate the potential of MM PBF-LB/M for particle-accelerator applications, an RFQ prototype was developed with a CuCr1Zr inner cavity and integrated tool-steel CF knife-edge flanges. The successful fabrication of the prototype, together with the helium leak-rate measurements, demonstrates the feasibility of this approach. In addition, the integrated cooling-channel geometry highlights the design advantages of PBF-LB/M compared with conventional RF cavity manufacturing. At the same time, the observed powder residues and their presumed impact on the helium leak-rate measurement, as well as the reduced quality factor caused by intrinsic surface roughness, illustrate typical challenges associated with PBF-LB/M. These limitations are considered addressable through

improved powder removal, process optimization, and suitable post-processing strategies, as already demonstrated for comparable geometries.

With the ongoing development of MM PBF-LB/M and the expected expansion of compatible material combinations, this technology offers substantial potential for functional particle-accelerator components. Potential candidates include multi-material components whose performance is limited, for example, by high thermal loads, such as crotch absorbers [32, 33], collimator jaws [34, 35], and particle or X-ray targets [36, 37].

ACKNOWLEDGEMENTS

This study is funded by the Federal Ministry of Research, Technology and Space (BMFTR) via the Project PosiLac (05K25WN1) and ERUM-Pro. In addition, the equipment used in this study, originating from the FLAB-3Dprint research project, is funded by dtec.bw—Research Center for Digitalization and Technology of the Bundeswehr. We would like to express our sincere gratitude for this support. dtec.bw is funded by the European Union—NextGenerationEU.

REFERENCES

[1] H. Hähnel *et al.*, "RF conditioning of an IH-DTL cavity made using additive manufacturing," in *Proc. IPAC'24*, Nashville, TN, USA, May 2024, paper THPR10, pp. 3495–3498. doi:10.18429/JACoW-IPAC2024-THPR10

[2] C. Zhang, R. Böhm, E. Boos, R. Cherif, A. Japs, and S. Wunderlich, "From concept to reality: Metal additive manufacturing in particle accelerator and storage ring R&D at GSI and for FAIR," *Eur. Phys. J. Spec. Top.*, pp. 1–19, 2026.

[3] M. Mayerhofer, J. Mitteneder, and G. Dollinger, "A 3D printed pure copper drift tube linac prototype," *Rev. Sci. Instrum.*, vol. 93, no. 2, p. 023304, 2022. doi:10.1063/5.0068494

[4] T. Romano *et al.*, "Metal additive manufacturing for particle accelerator applications," *Phys. Rev. Accel. Beams*, vol. 27, no. 5, p. 054801, 2024. doi:10.1103/PhysRevAccelBeams.27.054801

[5] M. Mayerhofer *et al.*, "Red and green laser powder bed fusion of pure copper in combination with chemical post-processing for RF cavity fabrication," *Instruments*, vol. 8, no. 3, p. 39, 2024. doi:10.3390/instruments8030039

[6] J. Guan and Q. Wang, "Laser powder bed fusion of dissimilar metal materials: A review," *Materials*, vol. 16, no. 7, p. 2757, 2023. doi:10.3390/ma16072757

[7] A. Kavousi Sisi *et al.*, "Functionally graded multi-materials by laser powder bed fusion: A review on experimental studies," *Prog. Addit. Manuf.*, vol. 10, pp. 1843–1912, 2025. doi:10.1007/s40964-024-00739-1

[8] C. Anstätt, "Multimaterialverarbeitung mittels Laserstrahlschmelzen am Beispiel von metallischen Verbindungen mit der Kupferlegierung CW106C," Ph.D. dissertation, Technische Universität München, Munich, Germany, 2020.

[9] S. Brenner *et al.*, "A radio-frequency quadrupole prototype additively manufactured as a multi-material component," *Prog. Addit. Manuf.*, vol. 10, pp. 3951–3961, 2025. doi:10.1007/s40964-025-01120-6

[10] H. Miao *et al.*, "Interfacial microstructure, element diffusion, mechanical properties and metallurgical bonding mechanism of 316L-AlSi10Mg multi-material parts fabricated by laser powder bed fusion," *J. Mater. Res. Technol.*, vol. 26, pp. 8351–8365, 2023. doi:10.1016/j.jmrt.2023.09.158

[11] T. Bareth, D. Eder, M. Lehmann, G. Schlick, and C. Seidel, "Multi-material additive manufacturing of conductor-insulator compounds for battery cell cap fabrication," *Mater. Des.*, vol. 254, p. 114010, 2025. doi:10.1016/j.matdes.2025.114010

[12] X. Wang *et al.*, "Formation of the Cu+Nb interlayer in the Inconel 718/Ti6Al4V multi-material obtained by selective laser melting," *Materials*, vol. 17, no. 23, p. 5801, 2024. doi:10.3390/ma17235801

[13] J. Walker, J. R. Middendorf, C. C. C. Lesko, and J. Gockel, "Multi-material laser powder bed fusion additive manufacturing in 3-dimensions," *Manuf. Lett.*, vol. 31, pp. 74–77, 2022. doi:10.1016/j.mfglet.2021.07.011

[14] H. Pasiowiec *et al.*, "Microstructure and mechanical properties of 316L/Inconel 625 gradient multi-material additively manufactured by laser powder bed fusion," *Mater. Des.*, vol. 260, p. 115162, 2025. doi:10.1016/j.matdes.2025.115162

[15] B. B. Ravichander, S. H. Jagdale, and G. Kumar, "Cost-effective and adaptable lab-scale multi-material system for LPBF," *Int. J. Adv. Manuf. Technol.*, vol. 137, no. 11–12, pp. 5585–5593, 2025. doi:10.1007/s00170-025-15495-x

[16] B. Rankouhi, Z. Islam, F. E. Pfefferkorn, and D. J. Thoma, "Characterization of multi-material 316L-Hastelloy X fabricated via laser powder-bed fusion," *Mater. Sci. Eng. A*, vol. 847, p. 142749, 2022. doi:10.1016/j.msea.2022.142749

[17] B. Guimaraes *et al.*, "WC-Co/316L stainless steel joining by laser powder bed fusion for multi-material cutting tools manufacturing," *Int. J. Refract. Met. Hard Mater.*, vol. 112, p. 106140, 2023. doi:10.1016/j.ijrmhm.2023.106140

[18] M. Oel *et al.*, "Multi-material laser powder bed fusion additive manufacturing of concentrated wound stator teeth," *Addit. Manuf. Lett.*, vol. 7, p. 100165, 2023. doi:10.1016/j.addlet.2023.100165

[19] Y.-H. Chueh, B.-Y. Hsieh, and A. J. Shih, "Interfacial characteristics in multi-material laser powder bed fusion of CuZr/316L stainless steel," *CIRP Ann.*, vol. 73, no. 1, pp. 145–148, 2024. doi:10.1016/j.cirp.2024.03.001

[20] L. Liu *et al.*, "Laser additive manufacturing of a 316L/CuSn10 multimaterial coaxial nozzle to alleviate spattering adhesion and burning effect in directed energy deposition," *J. Manuf. Process.*, vol. 82, pp. 51–63, 2022. doi:10.1016/j.jmapro.2022.07.038

[21] A. Cunha *et al.*, "420 stainless steel-Cu parts fabricated using 3D multi-material laser powder bed fusion: A new solution for plastic injection moulds," *Mater. Today Commun.*, vol. 32, p. 103852, 2022. doi:10.1016/j.mtcomm.2022.103852

[22] Y. Li *et al.*, "Interface microstructure and mechanical properties of IN625-CuCrZr multiple materials by selective laser melting," *Mater. Lett.*, p. 140695, 2026.

[23] Fraunhofer-Institut für Gießerei-, Composite- und Verarbeitungstechnik IGCV, "Additive Fertigung: Metall und Multimaterial," Fraunhofer IGCV, accessed May 15, 2026. https://www.igcv.fraunhofer.de/de/forschung/kompetenzen/multimaterial.html

[24] X. Yang *et al.*, "Interfacial characteristics and mechanical performance of IN718/CuSn10 fabricated by laser powder bed fusion," *Crystals*, vol. 15, no. 4, p. 344, 2025. doi:10.3390/cryst15040344

[25] A. Marques *et al.*, "Inconel 718-copper parts fabricated by 3D multi-material laser powder bed fusion: A novel technological and designing approach for rocket engine," *Int. J. Adv. Manuf. Technol.*, vol. 122, pp. 2113–2123, 2022. doi:10.1007/s00170-022-10011-x

[26] Z. Hu *et al.*, "Synchronized construction of metallurgical bonding and mechanical interlocking interface in immiscible W/CuCrZr functional gradient material by additive manufacturing," *Scripta Mater.*, vol. 260, p. 116599, 2025. doi:10.1016/j.scriptamat.2025.116599

[27] C. Wei, M. Liu, Y. Gu, Y. Huang, Q. Chen, Z. Li, and L. Li, "Multi-material additive-manufacturing of tungsten-copper alloy bimetallic structure with a stainless-steel interlayer and associated bonding mechanisms," *Addit. Manuf.*, vol. 50, p. 102574, 2022. doi:10.1016/j.addma.2021.102574

[28] D. Cheng *et al.*, "Additive manufacturing of lithium aluminosilicate glass-ceramic/metal 3D electronic components via multiple material laser powder bed fusion," *Addit. Manuf.*, vol. 49, p. 102481, 2022. doi:10.1016/j.addma.2021.102481

[29] M. Mayerhofer *et al.*, "First high quality drift tube Linac cavity additively manufactured from pure copper," in *Proc. IPAC'23*, Venice, Italy, May 2023, paper THPM035, pp. 4967–4970. doi:10.18429/JACoW-IPAC2023-THPM035

[30] X. Tang *et al.*, "A study on the mechanical and electrical properties of high-strength CuCrZr alloy fabricated using laser powder bed fusion," *J. Alloys Compd.*, vol. 924, p. 166627, 2022. doi:10.1016/j.jallcom.2022.166627

[31] A. Ratkus *et al.*, "Performance evaluation of additively manufactured pure copper radio frequency quadrupole by low-power RF and high-field gradient tests," in *Proc. IPAC'25*, Taipei, Taiwan, Jun. 2025, paper THPB051, pp. 2612–2615. doi:10.18429/JACoW-IPAC2025-THPB051

[32] I. C. Sheng *et al.*, "Design of TPS crotch absorber," in *Proc. IPAC'10*, Kyoto, Japan, May 2010, paper TUPEA079.

[33] M. Quispe *et al.*, "Development of the crotch absorbers for ALBA storage ring," in *Proc. MEDSI'08*, Saskatoon, Canada, 2008, pp. 1–15.

[34] J.-B. Yu *et al.*, "Thermal analysis and tests of W/Cu brazing for primary collimator scraper in CSNS/RCS," *Nucl. Sci. Tech.*, vol. 28, no. 4, p. 46, 2017. doi:10.1007/s41365-017-0208-9

[35] I. V. Leitão, "Development, validation and application of a novel method for estimating the thermal conductance of critical interfaces in the jaws of the LHC collimation system," in *Proc. IPAC'13*, Shanghai, China, May 2013, pp. 3430–3432.

[36] J. Busom Descarrega *et al.*, "Application of hot isostatic pressing (HIP) technology to diffusion bond refractory metals for proton beam targets and absorbers at CERN," *Mater. Des. Process. Commun.*, vol. 2, no. 1, p. e101, 2020. doi:10.1002/mdp2.101

[37] J. Winter *et al.*, "Heat management of a compact x-ray source for microbeam radiotherapy and FLASH treatments," *Med. Phys.*, vol. 49, no. 5, pp. 3375–3388, 2022. doi:10.1002/mp.15611